Orbital Structure and Magnetic Ordering in Layered Manganites:
Universal Correlation and Its Mechanism

S. Okamoto, S. Ishihara, and S. Maekawa

Institute for Materials Research, Tohoku University, Sendai 980-8577, Japan

(February 1, 2008)

Correlation between orbital structure and magnetic ordering in bilayered manganites is examined. A level separation between the $3d_{3z^2-r^2}$ and $3d_{x^2-y^2}$ orbitals in a Mn ion is calculated in the ionic model for a large number of the compounds. It is found that the relative stability of the orbitals dominates the magnetic transition temperatures as well as the magnetic structures. A mechanism of the correlation between orbital and magnetism is investigated based on the theoretical model with the two e_g orbitals under strong electron correlation.

PACS numbers: 75.30.Vn, 75.30.Kz, 71.10.-w, 75.80.+q

Since the discovery of the colossal magnetoresistance (CMR), studies of manganites with cubic perovskite structure have been renewed theoretically and experimentally. Competition and cooperation between spin, charge and orbital degrees of freedom as well as lattice cause the dramatic changes of transport and magnetic properties. Manganites with bilayered structure $A_{2-2x}B_{1+2x}Mn_2O_7$, where A and B are trivalent and divalent cations, respectively, are another class of CMR materials [1,2]. Since an extremely large MR is observed near the transition from paramagnetic (PM) insulator to ferromagnetic (FM) metal, it has been considered that several concepts proposed in the cubic compounds are applicable to the bilayered ones.

In cubic manganites, one of the key factors dominating the magnetic orderings is the tolerance factor [3]; a bending of a Mn-O-Mn bond decreases the hopping integral of carriers. As a result, the ferromagnetic transition temperature T_c decreases in the double exchange (DE) scenario. However, in bilayered manganites, the Mn-O-Mn bond angle is almost unchanged with changing cations and carrier concentration, as shown later, in spite of a wide variety of the magnetic structures. Various key factors dominating the magnetic ordering, which are not included in the DE model, were experimentally suggested, e.g. the antiferromagnetic (AFM) superexchange (SE) interaction [4], the local lattice distortion [5–8], the charge and orbital degrees of freedom and their orderings [9,10] and so on. However, systematics in their correlations for a variety of compounds and their mechanisms still remain to be clarified.

In this letter, we study the correlation between magnetic ordering and orbital structure in bilayered manganites. The two e_g orbitals, i.e. the $3d_{3z^2-r^2}$ and $3d_{x^2-y^2}$ orbitals in a Mn^{3+} ion split in the crystalline field of the bilayered structure and one of them is occupied by an electron. It is known that the occupied orbital controls the anisotropy of the magnetic interaction as well as its strength. The level separation between the orbitals is calculated in the ionic model for a large number of the compounds. We find a universal correlation between the

relative stability of the orbitals and the magnetic transition temperatures as well as the magnetic structures. A mechanism of the correlation is investigated based on the theoretical model with the e_g orbitals under strong electron correlation.

We first show that neither the tolerance factor nor the bond length governs T_C and the Néel temperature T_N for the A-type AFM ordering [11]. The tolerance factor in the bilayered crystals is defined by $t = (d_{O(1)-A(1)} + d_{O(2)-A(2)})/(2\sqrt{2}d_{Mn-O(3)})$ where d_{A-B} is a bond length between A and B ions. The position of each ion is shown in the inset of Fig. 1(a). Being based on the structural data obtained by the neutron and x-ray diffraction experiments [12–23], we evaluate t and the bond length between nearest neighboring (NN) Mn ions in the ab plane d^{ab}_{Mn-Mn} for a variety of compounds. T_C and T_N are plotted as functions of t and d^{ab}_{Mn-Mn} in Figs. 1 (a) and (b), respectively. Almost all t's are located in a narrow region where T_C's and T_N's are distributed randomly. In addition, T_C is not correlated with d^{ab}_{Mn-Mn}, either. Although T_N increases with increasing d^{ab}_{Mn-Mn}, this correlation is opposite to that predicted by the DE scenario where, with increasing the bond length, the hopping integral decreases and the FM interaction in the ab plane decreases. We conclude that the DE model, which includes the change of the hopping integral caused by the change of the bond angle/length, can not explain $T_{C(N)}$. We also examined correlations between $T_{C(N)}$ and a number of other quantities: the torelance factor evaluated by the ionic radius, a Mn-O(3)-Mn bond angle, a Mn-O(1)-Mn bond length, Mn-O bond lengths, a lattice spacing between NN bilayers, lattice constants and the valence-bond sum for a Mn ion. However, there are not clear correlations between these parameters and $T_{C(N)}$.

Let us focus on the correlation between $T_{C(N)}$ and a relative stability of the e_g orbitals. We employ the ionic model to examine the electronic energy-level structures. This model may be justified by the following considerations [24]: (1) the manganites at $x = 0$ are classified as charge-transfer type insulators in which the ionic model provides a good starting point [25]. (2) The
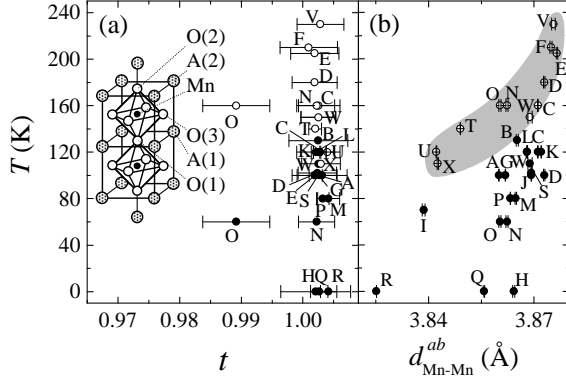
1

FIG. 1. T_C and T_N as functions of (a) t and $d^{ab}_{\text{Mn-Mn}}$. Filled and open circles indicate T_C and T_N, spectively. t and $d^{ab}_{\text{Mn-Mn}}$ are obtained from the structu data in the following compounds: A: La$_{1.4}$Sr$_{1.6}$Mn$_2$O$_7$ [12], B: La$_{1.3}$Sr$_{1.7}$Mn$_2$O$_7$ (p) [12], C: La$_{1.2}$Sr$_{1.8}$Mn$_2$O$_7$ [12], D: La$_{1.1}$Sr$_{1.9}$Mn$_2$O$_7$ (s) [12], E: La$_{1.04}$Sr$_{1.96}$Mn$_2$O$_7$ [12], F: LaSr$_2$Mn$_2$O$_7$ (s) [12], G: La$_{1.4}$Sr$_{1.6}$Mn$_2$O$_7$ (p) [13], Pr$_{1.4}$Ca$_{1.3}$Ba$_{0.3}$Mn$_2$O$_7$ (p) [14], I: Nd$_{1.4}$Ca$_{1.6}$Mn$_2$O$_7$ (p) [J: La$_{1.4}$Sr$_{1.6}$Mn$_2$O$_7$ (p) [15], K: La$_{1.2}$Sr$_{1.8}$Mn$_2$O$_7$ (p) [16], La$_{1.2}$Sr$_{1.8}$Mn$_2$O$_7$ (s) [17], M: La$_{1.2}$(Sr$_{0.8}$ Ca$_{0.2}$)$_{1.8}$Mn$_2$O$_7$ [17], N: La$_{1.2}$(Sr$_{0.7}$ Ca$_{0.3}$)$_{1.8}$Mn$_2$O$_7$ (s) [17], O: La$_{1.2}$(S Ca$_{0.4}$)$_{1.8}$Mn$_2$O$_7$ (p) [17], P: (La$_{0.8}$Nd$_{0.2}$)$_{1.2}$Sr$_{1.8}$Mn$_2$O$_7$ [17], Q: (La$_{0.6}$Nd$_{0.4}$)$_{1.2}$Sr$_{1.8}$Mn$_2$O$_7$ (s) [17], R: Sm$_{1.2}$S Mn$_2$O$_7$ (p) [18], S: La$_{1.2}$Sr$_{1.4}$Ca$_{0.4}$Mn$_2$O$_7$ (p) [19], NdSr$_2$Mn$_2$O$_7$ (p) [20], U: Nd$_{1.1}$Sr$_{1.9}$Mn$_2$O$_7$ (p) [20], LaSr$_2$Mn$_2$O$_7$ (p) [21], W: LaSr$_{1.6}$Ca$_{0.4}$Mn$_2$O$_7$ (p) [22], NdSr$_2$ Mn$_2$O$_7$ (s) [22] where (s) and (p) indicate the s gle and polycrystalline samples, respectively. The inset of shows a schematic picture of the bilayered structure.

ionic property is predominant between bilayers. (3) T energy-level structure given by band-structure calcu tions shows the same tendency with those by the ionic model [6,26]. The energy levels of the e_g orbitals split due to the electrostatic potential and one of the orbitals is occupied by an electron in a Mn^{3+} ion.

By using a large number of the structural data [12–23], we calculate the Madelung potential for a hole in the $3d_{3z^2-r^2}$ and $3d_{x^2-y^2}$ orbitals at site j defined by

$$V_{3z^2-r^2} = \frac{1}{2}\{V(\vec{r}_j + r_d\hat{z}) + V(\vec{r}_j - r_d\hat{z})\}, \qquad (1)$$

and

$$V_{x^2-y^2} = V(\vec{r}_j + r_d\hat{x}), \qquad (2)$$

respectively [27]. Here, $V(\vec{r}_j)$ is given by

$$V(\vec{r}_j) = \sum_{i\neq j} \frac{Z_i e^2}{|\vec{r}_j - \vec{r}_i|}, \qquad (3)$$

with a point charge $Z_i e$ at site i and the position $\vec{r}_i$ of the site. $r_d(=0.42\text{Å})$ is the radius of a Mn $3d$ orbital where its radial charge density becomes maximum [28] and $\hat{z}(\hat{x})$
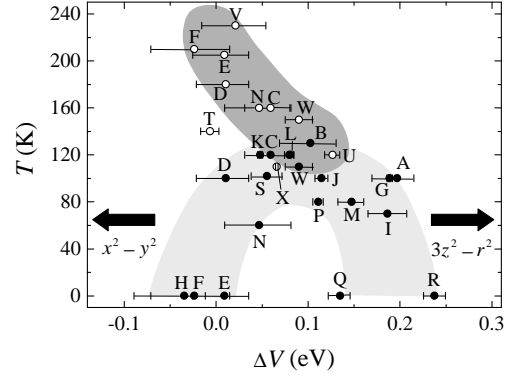

FIG. 2. T_C and T_N as functions of ΔV. Filled and open circles indicate T_C and T_N, respectively. ΔV's are calculated for the same compounds in Fig. 1. Note that in the region with large positive (negative) ΔV, the $3d_{3z^2-r^2}$ ($3d_{x^2-y^2}$) orbital is occupied by an electron.

is the unit vector in the $z(x)$ axis. The Ewald method is used for the lattice summation. Z_i's for Mn and O ions and a cation at A site are chosen to be $3 + x$, -2 and $(8 - 2x)/3$, respectively. The difference of the potentials

$$\Delta V = V_{3z^2-r^2} - V_{x^2-y^2}, \qquad (4)$$

represents the relative stability of the orbitals; with increasing ΔV, the energy level of the $3d_{3z^2-r^2}$ orbital for an electron relatively decreases.

T_N and T_C are plotted as functions of ΔV in Fig. 2 where the structural data at room temperature are used. Broad shades are drawn by considering experimental errors. It is clearly shown that both T_C and T_N are correlated with ΔV; T_N increases with decreasing ΔV and there is an optimal value of $\Delta V(\sim 0.08$ eV) for T_C. We estimate the strength of the correlation between T_N and ΔV by using the correlation coefficient: $r = \frac{1}{N}\sum_l (T_{Nl} - \overline{T_N})(\Delta V_l - \overline{\Delta V})/(\sigma_{T_N}\sigma_{\Delta V})$ where l indicates a sample and N is the number of samples. $\overline{\Delta V}$ ($\overline{T_N}$) and $\sigma_{\Delta V}$ (σ_{T_N}) are the mean value and the standard deviation of ΔV (T_N), respectively. We obtain $r = -0.89 \pm 0.11$ for single crystal samples and $r = -0.15 \pm 0.04$ for all samples including polycrystals. One might think that the $T_{C(N)}$ v.s. ΔV curve in Fig. 2 just reflects the relation between $T_{C(N)}$ and x in La$_{2-2x}$Sr$_{1+2x}$Mn$_2$O$_7$ (LSMO) [12,7]. However, when we pay attention to $T_{C(N)}$'s for samples with the same x (e.g., the samples C and K-R), we notice that the correlation remains. The correlation between T_N and ΔV explains that between T_N and $d^{ab}_{\text{Mn-Mn}}$ shown in Fig. 1(b), since ΔV is a decreasing function of $d^{ab}_{\text{Mn-Mn}}$ in the region, 3.84Å $< d^{ab}_{\text{Mn-Mn}} <$3.88Å.

In Fig. 3, we present the magnetic phase diagram at $T = 0$ as a function of ΔV and x. The structural data at room temperature are used. Symbols connected by dotted lines correspond to a series of LSMO with
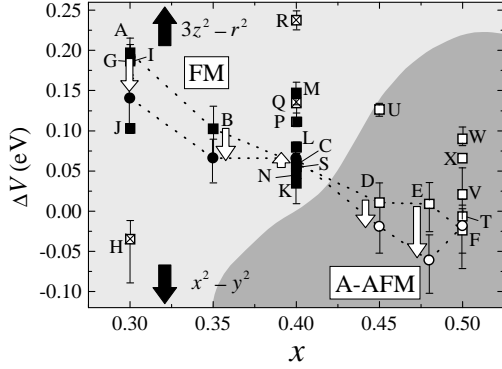
FIG. 3. The magnetic phase diagram at $T = 0$ as function of ΔV and x. Filled, open and crossed squares indicate the FM, A-type AFM and PM samples, respectively. ΔV's for filled and open circles are obtained from the data below T_C and T_N, respectively. Symbols connected by dotted lines indicate a series of LSMO. Bold arrows show $\delta(\Delta V) = \Delta V(T < T_{C(N)}) - \Delta V(T > T_{C(N)})$. ΔV's are calculated for the same compounds in Fig. 1. Note that the region with large positive (negative) ΔV, the $3d_{3z^2-}$ ($3d_{x^2-y^2}$) orbital is occupied by an electron.

$x = 0.3 - 0.5$ [12]. In addition, ΔV's calculated by using the data below $T_{C(N)}$ in LSMO are also plotted. Bold rows indicate the change of the Madelung potential with changing temperature from $T > T_{C(N)}$ to $T < T_{C(N)}$:

$$\delta(\Delta V) \equiv \Delta V(T < T_{C(N)}) - \Delta V(T > T_{C(N)}).$$

We find that the magnetic structures are governed by ΔV and x; the FM (A-type AFM) phase is located in the region with smaller (larger) x and moderate (smaller) ΔV. Let us focus on $\delta(\Delta V)$ in LSMO. $\delta(\Delta V)$'s are negative at $x = 0.3$ and 0.35. The absolute value of $\delta(\Delta V)$ gradually decreases with increasing x and $\delta(\Delta V)$ becomes a small positive value at $x = 0.4$. Below T_C, ΔV seems to approach to the optimal value of $\Delta V \sim 0.08$ where T_C becomes maximum as seen in Fig. 2. On the other hand, $\delta(\Delta V)$'s are negative at $x=0.45$ and 0.48 where the A-type AFM structure appears. The orbital structure and its stability in the FM phase have been studied by measuring the striction in Ref. [10]. The difference of the Mn-O bond lengths between PM and FM states was reported in Ref. [7]. These experimental results are consistent with the present results of $\delta(\Delta V)$ in Fig. 3.

Now we theoretically investigate a mechanism of the correlation between magnetic ordering and orbital structure. We start with the following Hamiltonian [27,29,30]:

$$\mathcal{H} = \mathcal{H}_t + \mathcal{H}_J + \mathcal{H}_H + \mathcal{H}_{AF} + \mathcal{H}_z. \tag{6}$$

Instead of the bilayered structure, the simple tetragonal lattice consisting of Mn ions is considered. In this model, the magnetic structure with FM and AFM alignments perpendicular and parallel to the c axis, respectively, corresponds to the A-type AFM structure [11]. In each Mn
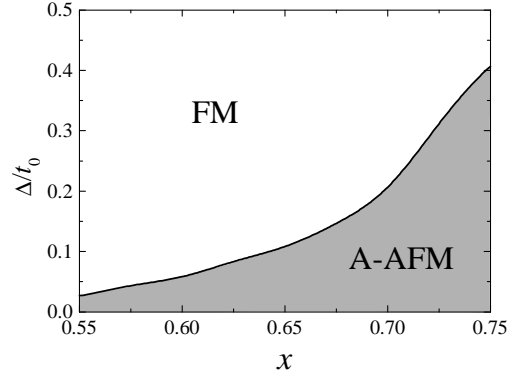

FIG. 4. The calculated magnetic phase diagram at $T = 0$ as a function of Δ and x. Note that in the region with large positive (negative) Δ, the $3d_{3z^2-r^2}$ ($3d_{x^2-y^2}$) orbital is occupied by an electron.

ion, the two e_g orbitals are introduced and the t_{2g} electrons are treated as a localized spin with $S = 3/2$. The first two terms in Eq. (6) correspond to the so-called t- and J-terms in the tJ model, respectively, with the two e_g orbitals under strong electron correlation. The third and fourth terms describe the Hund coupling between e_g and t_{2g} spins and the AFM SE interaction between t_{2g} spins, respectively. The splitting of the energy levels between $3d_{3z^2-r^2}$ and $3d_{x^2-y^2}$ orbitals is represented by the last term: $\mathcal{H}_z = -\Delta \sum_i T_{iz}$ where the pseudospin operator is given by $\vec{T}_i = \frac{1}{2} \sum_{\gamma\gamma'\sigma} d^\dagger_{i\gamma\sigma} \vec{\sigma}_{\gamma\gamma'} d_{i\gamma'\sigma}$ with $d_{i\gamma\sigma}$ being the annihilation operator of an e_g electron at site i with spin σ and orbital γ. The $+(-)$ eigenstate of T_{iz} corresponds to the state where the $3d_{3z^2-r^2}$ ($3d_{x^2-y^2}$) orbital is occupied by an electron. The anisotropies of the hopping integral and the SE interactions due to the layered structure are considered. The explicit expression and derivation of the Hamiltonian are presented in Refs. [27] and [29].

The calculated magnetic phase diagram at $T = 0$ is presented in Fig. 4 [30,31] where the mean field approximation is adopted. We note that the phase diagram derived in this approximation explains that in the cubic manganites [32]. The characteristic features shown in Fig. 3 are well reproduced by the present theory; the A-type AFM phase appears in the region with higher x and smaller Δ than that of the FM one. The range of the horizontal axis in Fig. 4 is larger than that in Fig. 3 by about 0.25. This discrepancy may be attributed to the neglect of the orbital fluctuation [33]. However, the characteristics of the phase diagram are insensitive to the parameters in the model. In the FM (A-type AFM) phase, the orbitals are uniformly aligned with $0 < \theta < 0.72\pi$ ($0.72\pi < \theta < \pi$) where θ describes the orbital state as $|\theta\rangle = \cos(\frac{\theta}{2})|3d_{3z^2-r^2}\rangle - \sin(\frac{\theta}{2})|3d_{x^2-y^2}\rangle$. The present results suggest that a dimensionality of the FM interaction is controlled by the orbital structure; in the A-type AFM phase, the FM ordering in the ab plane is caused by the

3

DE interaction, while the AFM in the c direction is by the AFM SE. When the $3d_{x^2-y^2}$ orbital is stabilized, the DE interaction in the ab plane (c direction) becomes strong (weak) and the A-type AFM phase appears [34]. A mixing of the orbitals is essential in the FM phase where the FM interaction overcomes the AFM SE one in the three directions. We note that, in Fig. 4, the FM phase appears not around $\Delta = 0$ but in a region of $\Delta > 0$, since the anisotropy in the hopping integral due to the layered structure stabilizes the $3d_{x^2-y^2}$ orbital more than $3d_{3z^2-r^2}$. It is worth to mention the change of the orbital structure associated with the magnetic ordering: By utilizing the mean filed approximation at finite temperature, we compare the orbital structures above and below the magnetic transition temperatures. It is found that (1) there is an optimal mixing of the orbitals for the FM state and the orbital structure tends to approach to this structure below T_C and (2) the $3d_{x^2-y^2}$ orbital structure is stabilized below T_N. The theoretical results are consistent with $\delta(\Delta V)$'s shown in Fig. 3 by considering that the change of ΔV associated with the magnetic ordering is caused by that of the orbital structure.

In summary, we examine correlation between magnetic ordering and orbital structure in bilayered manganites. A relative stability of the e_g orbitals is investigated by calculating the Madelung potentials in a large number of the bilayered compounds. We find that the A-type AFM structure and the $3d_{x^2-y^2}$ orbital one are stabilized co-operatively and there is an optimal mixing between the $3d_{3z^2-r^2}$ and $3d_{x^2-y^2}$ orbitals for the FM ordering. A theory with the two e_g orbitals under strong electron correlation explains a mechanism of the universal correlation between orbital and magnetism.

[1] Y. Moritomo *et al.*, Nature (London) **380**, 141 (1996).
[2] T. Kimura *et al.*, Science **274**, 1698 (1996).
[3] H. Y. Hwang *et al.*, Phys. Rev. Lett. **75**, 914 (1995).
[4] T. G. Perring *et al.*, Phys. Rev. Lett. **78**, 3197 (1997).
[5] D. Louca *et al.*, Phys. Rev. Lett. **80**, 3811 (1998).
[6] D. S. Dessau *et al.*, Phys. Rev. Lett. **81**, 192 (1998).
[7] M. Medarde *et al.*, Phys. Rev. Lett. **83**, 1223 (1999).
[8] L. Vasiliu-Doloc *et al.*, Phys. Rev. Lett. **83**, 4393 (1999).
[9] Y. Moritomo *et al.*, Phys. Rev. B **56**, R7057 (1997).
[10] T. Kimura *et al.*, Phys. Rev. Lett. **81**, 5920 (1998).
[11] The following two layered AFM structures have been observed [12,13]: AFM-I consisting of the FM spin ordering in the plane and the AFM (FM) one along the c axis within (between NN) bilayers, and AFM-II consisting of the FM in the plane and the FM (AFM) along the c axis within (between NN) bilayers. Since the intrabilayer magnetic coupling is much larger than the interbilayer one [35], we term the AFM-I structure the A-type AFM one and regard the AFM-II as the FM.
[12] M. Kubota *et al.*, cond-mat/9902288.
[13] D. N. Argyriou *et al.*, Phys. Rev. B **59**, 8695 (1999).
[14] P. Laffez *et al.*, J. Appl. Phys. **80**, 5850 (1996).
[15] E.-O. Chi *et al.*, Phys. Rev. B **60**, 12 867 (1999).
[16] D. N. Argyriou *et al.*, Phys. Rev. Lett. **78**, 1568 (1997).
[17] T. Akimoto *et al.*, Phys. Rev. B **59**, R14 153 (1999).
[18] P. D. Battle *et al.*, J. Appl. Phys. **83**, 6379 (1998).
[19] C. H. Shen *et al.*, J. Appl. Phys. **86**, 2178 (1999).
[20] P. D. Battle *et al.*, Phys. Rev. B **54**, 15 967 (1996).
[21] R. Seshadri *et al.*, Solid State Commun. **101**, 453 (1997).
[22] T. Akimoto *et al.*, (unpublished).
[23] For the samples G, J, R, T and U where the two chemically distinct phases are observed, the structural data of the major phase are adopted.
[24] Y. Ohta *et al.*, Phys. Rev. B **43**, 2968 (1991).
[25] T. Arima *et al.*, Phys. Rev B **48**, 17 006 (1993).
[26] P. K. de Boer *et al.*, Phys. Rev. B **60**, 10 758 (1999).
[27] S. Ishihara *et al.*, J. Phys. Soc. Jpn. **66**, 2965 (1997).
[28] J. C. Slater in *Quantum Theory of Atomic Structure* (Mc-Graw Hill, New York, 1960) Vol. 1.
[29] S. Ishihara *et al.*, Physica C **263**, 130 (1996), and Phys. Rev. B **55**, 8280 (1997).
[30] In the Hamiltonian, we consider the SE interactions $J_{1,2}^{ab(c)}$ between e_g electrons, the AFM SE one $J_{AF}^{ab(c)}$ between t_{2g} spins and the hopping integral $t_0^{ab(c)}$ of e_g electrons where the subscript ab (c) indicates the interaction in the ab plane (the c direction) [27,29]. These values are chosen as $J_{1(2)}^{ab}/t_0^{ab} = 0.25$ (0.075), $J_{AF}^{ab}/t_0^{ab} = 0.002$ and $t_0^{ab}/t_0^c = \sqrt{J_{1,2}^{ab}/J_{1,2}^c} = \sqrt{J_{AF}^{ab}/J_{AF}^c} = 1.5$ in the numerical calculation. t_0^{ab} is represented as t_0 for simplicity.
[31] The phase diagram at $T = 0$ for the bilayered manganites has also been studied in the Hartree-Fock theory by R. Maezono and N. Nagaosa, cond-mat/9904427.
[32] S. Okamoto *et al.*, Phys. Rev. B **61**, (2000), and Y. Endoh *et al.*, Phys. Rev. Lett. **82**, 4328 (1999).
[33] S. Ishihara *et al.*, Phys. Rev. B **56**, 686 (1997).
[34] R. Maezono *et al.*, Phys. Rev. B **57**, R13 993 (1998).
[35] H. Fujioka *et al.*, J. Phys. Chem. Solids **60**, 1165 (1999).